Aqueous divalent metal–nitrate interactions: hydration *versus* ion pairing†

Man Xu,[a] James P. Larentzos,[b] Mazen Roshdy,[a] Louise J. Criscenti*[b] and Heather C. Allen*[a]

Received 25th April 2008, Accepted 24th June 2008
First published as an Advance Article on the web 15th July 2008
DOI: 10.1039/b807090n

Nitrate aqueous solutions, $Mg(NO_3)_2$, $Ca(NO_3)_2$, $Sr(NO_3)_2$, and $Pb(NO_3)_2$, are investigated using Raman spectroscopy and free energy profiles from molecular dynamics (MD) simulations. Analysis of the in-plane deformation, symmetric stretch, and asymmetric stretch vibrational modes of the nitrate ions reveal perturbation caused by the metal cations and hydrating water molecules. Results show that Pb^{2+} has a strong tendency to form contact ion pairs with nitrate relative to Sr^{2+}, Ca^{2+}, and Mg^{2+}, and contact ion pair formation decreases with decreasing cation size and increasing cation charge density: $Pb^{2+} > Sr^{2+} > Ca^{2+} > Mg^{2+}$. In the case of Mg^{2+}, the Mg^{2+}–OH_2 intermolecular modes indicate strong hydration by water molecules and no contact ion pairing with nitrate. Free energy profiles provide evidence for the experimentally observed trend and clarification between solvent-separated, solvent-shared, and contact ion pairs, particularly for Mg^{2+} relative to other cations.

1. Introduction

Ion pairing, the association of oppositely charged ions in electrolyte solutions to form distinct chemical species, ion pairs, is of prime importance in many areas including solution chemistry, atmospheric chemistry, geochemistry, and biology.[1–5] Ion pairs are classified into three types: solvent-separated ion pairs where the primary solvation shells of the cation and the anion remain intact, solvent-shared ion pairs where a single solvent layer exists between the cation and the anion, and contact ion pairs where no solvent exists between the ion partners of the pair, and ions are in direct contact.[1,6] Ion pairing in systems containing nitrate anion, one of the most abundant anions in atmospheric aerosols, has attracted considerable interest.[7–13] The formation of ion pairs with a counter cation changes the environment of the nitrate anion. This has implications for surface reactivity and reaction mechanisms in atmospheric and geochemical systems.

Aqueous solutions of divalent metal cations and nitrate anions have received special attention due to the fact that ion pair formation between nitrate anions and doubly charged cations is highly possible. Numerous studies have been conducted to investigate ion pairing in nitrate aqueous solutions, mainly focusing on individual metal–nitrate salts and the effects of concentration, temperature, and solvent.[5,11,12,14–18] Few studies[4,19–21] have been conducted to understand the relative differences in varying the type of counter cation.

We are interested in understanding ion pairing phenomena in aqueous media and at the air–aqueous interface inclusive of understanding hydrogen bonding and water structure. In this paper, we present a comprehensive study of ion pairing between divalent metal and nitrate in aqueous solutions by combining Raman spectroscopy and free energy profiles from molecular dynamics (MD) simulations. Two manuscripts in preparation[22,23] explore divalent metal ions and nitrate ions in addition to interfacial water structure in these systems at the air–aqueous interface. In this work, we elucidate effects of different metal cations, Mg^{2+}, Ca^{2+}, Sr^{2+}, and Pb^{2+}, on metal–nitrate ion pairing spectroscopically and thermodynamically in aqueous solution. A series of nitrate solutions, from low concentrations to saturated concentrations at room temperature, are investigated using Raman spectroscopy. Ammonium nitrate solutions that give little indication of disturbance of the nitrate anion by the cation[24] are studied for comparison. The spectral features of nitrate vibrational modes indicate that Pb^{2+} has a strong tendency to form ion pairs with nitrate anions, and the formation of contact ion pairs decreases with decreasing cation size and increasing cation surface charge density. The effects of Mg^{2+} cations on ion paring are significantly different relative to other cations. The intermolecular stretching modes Mg^{2+}–OH_2 observed in the $Mg(NO_3)_2$ aqueous solutions follow a linear relationship with the $Mg(NO_3)_2$ concentration, revealing no contact ion pair formation between Mg^{2+} cations and nitrate anions. Potential-of-mean-force MD simulations provide molecular-scale insight into the thermodynamically favorable complexes. The free energy profiles show that contact ion pairing in aqueous $Mg(NO_3)_2$ is thermodynamically unfavorable, whereas in $Ca(NO_3)_2$, $Sr(NO_3)_2$, and $Pb(NO_3)_2$ the formation of contact

[a] *Department of Chemistry, The Ohio State University, 100 W. 18th Avenue, Columbus, Ohio 43210. E-mail: allen@chemistry.ohio-state.edu*
[b] *Sandia National Laboratories, P.O. Box 5800, MS 0754, Albuquerque, NM 87185. E-mail: ljcrisc@sandia.gov*

† Electronic supplementary information (ESI) available: Curve-fitting results, infrared spectra of nitrate symmetric stretching modes, and Raman spectra of $NaNO_3$ aqueous solutions. For ESI see DOI: 10.1039/b807090n

ion pairs is preferred over solvent-shared and solvent-separated ion pairing.

2. Experimental

Raman instrumentation

The Raman experimental setup used for obtaining vibrational spectra of nitrate consists of a 785 nm continuous wave laser (Raman System Inc), a 7.5 mm focusing Raman probe (InPhotonics, RPS785/12-5), a 500 mm monochromator (Acton Research, SpectroPro SP-500) using a 600 groove mm^{-1} grating blazed at 1 μm, and a liquid nitrogen cooled charge-coupled device (CCD) camera (Roper Scientific, LN400EB, 1340 × 400 pixel array, back-illuminated and deep depletion CCD). The collection fiber optic, which is part of the InPhotonics Raman probe, was coupled to the entrance slit of the monochromator. The slit width was set to 50 μm, and the resolution, determined experimentally, was 3.2 cm^{-1} (reported as the full width at half maximum (fwhm)). The power of the 785 nm beam for sample illumination was ~240 mW. Spectra were collected with an exposure time of 50 s unless otherwise noted.

Raman spectra of intermolecular vibrational modes shown in Fig. 6 were obtained by passing an unpolarized 532 nm light (Spectra-Physics, Millennia II) from a continuous wave laser onto the sample using a 5 mm focusing Raman probe (InPhotonics, RPS532/12-10). The Raman scatter was focused onto the entrance slit of a 500 mm monochromator (Acton Research, SpectroPro SP-500) with a BK7 lens (focal length 75 mm). A long-pass 535 nm filter (Omega Optical, Custom) was placed in the light path before the monochromator to remove the 532 nm light. The Raman scatter was dispersed by a 1200 groove mm^{-1} grating blazed at 1 μm, and collected on a liquid nitrogen cooled CCD camera (Roper Scientific, LN400EB). The power of the 532 nm beam for sample illumination was ~170 mW, and the slit width of the monochromator entrance slit was set to 100 μm. These Raman spectra were collected with an exposure time of 5 min.

For all Raman experiments, the monochromator was calibrated using the 435.833 nm Hg line of a fluorescent light before data collection. The calibration of the wavenumber position was completed by taking Raman spectra of naphthalene and comparing peak positions with literature values.[25] Raman spectra were obtained at a room temperature of 23 ± 1 °C.

Chemicals

All nitrate salts, $Mg(NO_3)_2{\cdot}6H_2O$ (Certified ACS, 98.0–02.0%), $Ca(NO_3)_2{\cdot}4H_2O$ (Certified ACS, 99.0–103.0%), $Sr(NO_3)_2$ (Certified ACS, 99.0%), and $Pb(NO_3)_2$ (Certified ACS, 99.0%) were purchased from Fisher Scientific and were used as received. The aqueous solutions were made using Nanopure water with a resistivity of 18.0–18.3 MΩ cm. Molality (m), which is defined as the moles of solute per kg of water, is used as the concentration unit for the nitrate salt solutions in this paper. Mole fraction (x) values are placed in parentheses next to the molality throughout the text for reference. Molarity (M) has been used for specific analyses since the Raman probes a set volume. Table 1 shows the concentration unit conversions, molality (m), mole fraction (x), and molarity (M).

Computational methods

To investigate the relative energetics of metal–nitrate complexation, potential-of-mean-force (PMF) calculations[26,27] were conducted to obtain free energy profiles of $MgNO_3^+$, $CaNO_3^+$, $SrNO_3^+$, and $PbNO_3^+$ at infinite dilution. The potential of mean force, W, between the metal (M) and nitrate (NO_3) was calculated by integrating the total metal–nitrate mean force $F(r)$:

$$W(r) = W(r_o) - \int_{r_o}^{r} F(r)\mathrm{d}r$$

where, in an infinite system, $r_o \rightarrow \infty$. In a finite system, the standard practice is to assume that the continuum limiting behavior $W(r_o) \approx (q_M q_{NO_3}/\varepsilon r_o)$, where r_o is chosen such that $W(r_o)$ is small relative to $W(r)$. For our calculations, we chose r_o to be 10.0 Å, a distance similar to that selected by other researchers.[27–29]

To calculate the PMF for each metal–nitrate pair, a series of 61 canonical ensemble (NVT) MD simulations were conducted for 1 ns at 300 K on a neutral 25 Å × 25 Å × 25 Å simulation cell containing 512 water molecules, one divalent metal cation, and two nitrate anions. The separation distance between the cation and the nitrogen atom of one nitrate anion was constrained *via* the SHAKE algorithm[30] to distances between 1.0 Å and 10.0 Å, incrementing by 0.15 Å. The constrained nitrate anion had full rotational symmetry. The second nitrate anion was unconstrained and moved freely within the simulation cell. The constraint force between the cation and the anion was collected every timestep (dt = 0.5 fs) over the duration of each MD simulation and integrated to give the free energy profile (or mean force profile).[26]

All simulations were performed within the canonical ensemble using the LAMMPS software package.[31,32] A Nose–Hoover thermostat with a relaxation time of 0.1 ps was used to maintain the average temperature of 300 K. The flexible simple point charge (SPC) water model[33,34] was used in conjunction with cation force field parameters derived to match hydration free energies[35] and nitrate force field parameters derived to match the vibrational frequencies in the gas phase.[36] Long range electrostatic interactions were handled using the Ewald summation method and the van der Waals interactions were modeled through a 12-6 Lennard-Jones potential. All cross-parameters were computed through Lorentz–Berthelot combining rules.

3. Results and discussion

3.1 Raman spectroscopy

Raman spectra were obtained from aqueous solutions of metal–nitrate salts that ranged from 0.10 m (0.0018 x) to highly concentrated solutions at room temperature. The highly concentrated solutions approach the solubility limit of the salts. The Raman spectra of concentrated $Mg(NO_3)_2$, $Ca(NO_3)_2$, $Sr(NO_3)_2$, and $Pb(NO_3)_2$ solutions are shown in

Table 1 Concentrations of the nitrate aqueous solutions

Molality, m/moles per kg of water	Salt mole fraction, x	Number of water molecules per ion	Molarity, M/moles per litre			
			$Mg(NO_3)_2$	$Ca(NO_3)_2$	$Sr(NO_3)_2$	$Pb(NO_3)_2$
0.10	0.0018	185	0.089	0.092	0.10	0.10
0.50	0.0089	37	0.47	0.46	0.49	0.49
1.0	0.018	18	0.88	0.90	0.96	0.94
1.7	0.030	11	1.3	1.4	1.6	1.6
3.3	0.056	5.6	2.2	2.3	2.7	—
4.9	0.081	3.8	2.8	—	—	—
5.1	0.084	3.6	—	3.2	—	—

Fig. 1. Fig. 1a shows the Raman spectra of the intermolecular metal–water vibrational modes, which is discussed in section 3.1.4. In Fig. 1b, there are three vibrational modes of nitrate ions: in-plane deformation (IPD) modes at $\sim$719 cm^{-1}, symmetric stretching (SS) modes at $\sim$1049 cm^{-1} (also shown in the inset of Fig. 1), and asymmetric stretching (AS) modes at $\sim$1370 cm^{-1}.[21,37,38] In the $Mg(NO_3)_2$ aqueous solution, the nitrate IPD occurs as a well defined single peak, whereas peak splitting or an asymmetric peak shape of the IPD is observed for $Ca(NO_3)_2$, $Sr(NO_3)_2$, and $Pb(NO_3)_2$. For the nitrate SS modes shown in Fig. 1 and the inset, the frequency differences between $Pb(NO_3)_2$ and other aqueous solutions of divalent cations and nitrate anions are observed. In the case of the AS modes, small variations are observed for different nitrate saturated solutions.

The spectral features of the nitrate vibrational bands arise from the symmetry changes of nitrate. Unperturbed nitrate ion has a D_{3h} symmetry and is expected to exhibit a four-band spectrum:[21,37,38] SS band $\nu_1(A_1')$ at $\sim$1049 cm^{-1}, out-of-plane deformation (OPD) band $\nu_2(A_2'')$ at $\sim$830 cm^{-1}, AS $\nu_3(E')$ at $\sim$1370 cm^{-1}, and IPD $\nu_4(E')$ at $\sim$719 cm^{-1}. The AS and IPD modes are both Raman and IR active, while the SS mode is Raman active only and the OPD is IR active only. In aqueous solutions, the perturbation from metal cations and water molecules causes a lowering of symmetry of the nitrate group from D_{3h} to C_{2v} or C_s, resulting in more vibrational bands.[14,21,37] Vibrational bands in the SS and OPD regions become both Raman and IR active, with frequencies similar to those of unperturbed nitrate. Two bands in the AS region arise from the lifting of degeneracy of the AS band, and two bands in the IPD region arise from the lifting of degeneracy of the IPD band. These are in accord with the results of our Raman (Fig. 1) and infrared (electronic supplementary information, ESI)† spectra. For example, the SS band occurs in the infrared spectra of our metal–nitrate solutions (ESI).† Two AS bands at $\sim$1345 cm^{-1} and $\sim$1420 cm^{-1} are observed in the Raman spectra of the nitrate aqueous solutions. Two IPD bands instead of one IPD band are present in the Raman spectra of $Ca(NO_3)_2$, $Sr(NO_3)_2$, and $Pb(NO_3)_2$ solutions. Although with changes of symmetry, the OPD band is not observed as is expected. In the following paragraphs, the spectral changes of the IPD, the SS, the AS as well as the intermolecular metal–water bands are discussed in detail.

3.1.1 In-plane deformation. The splitting of the nitrate IPD band has been used as a criterion for contact ion pair formation.[4,19,38–40] The Raman spectra of the nitrate IPD modes of NH_4NO_3, $Mg(NO_3)_2$, $Ca(NO_3)_2$, $Sr(NO_3)_2$ and $Pb(NO_3)_2$ are shown in Fig. 2. In the spectra of NH_4NO_3 aqueous solutions (Fig. 2a), from concentration 0.20 m (0.036 x) to 20 m (0.26 x), neither peak splitting nor frequency shift is observed. It is important to note that in concentrated NH_4NO_3 aqueous solutions, for instance, at concentration 20 m (0.26 x), there are only 1.4 water molecules per ion, and therefore the direct contact between NH_4^+ and NO_3^- must occur. However, almost no peak splitting or shifting is observed according to

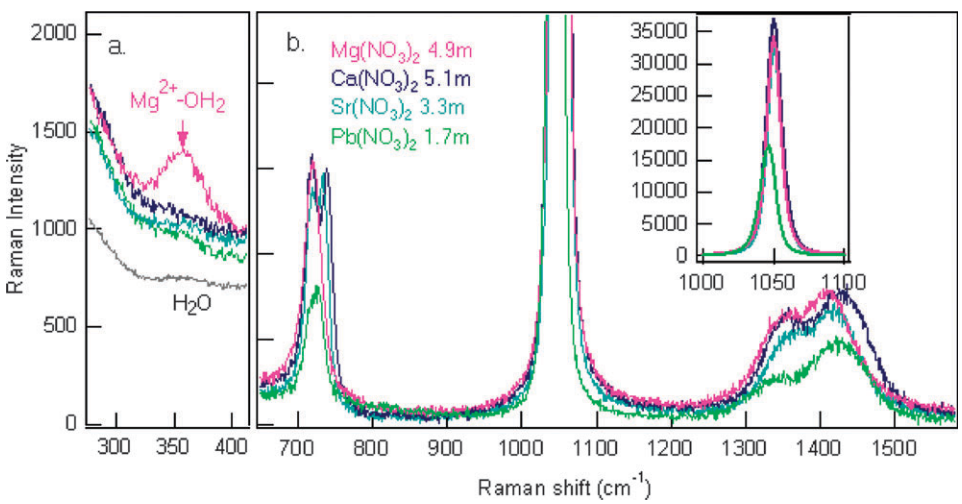

Fig. 1 Raman spectra of concentrated aqueous solutions (salt solubility limits the concentrations) of $Mg(NO_3)_2$, $Ca(NO_3)_2$, $Sr(NO_3)_2$, and $Pb(NO_3)_2$: (a) intermolecular vibrational modes; (b) nitrate vibrational modes. Inset of (b): Raman spectra of the nitrate symmetric stretch modes.

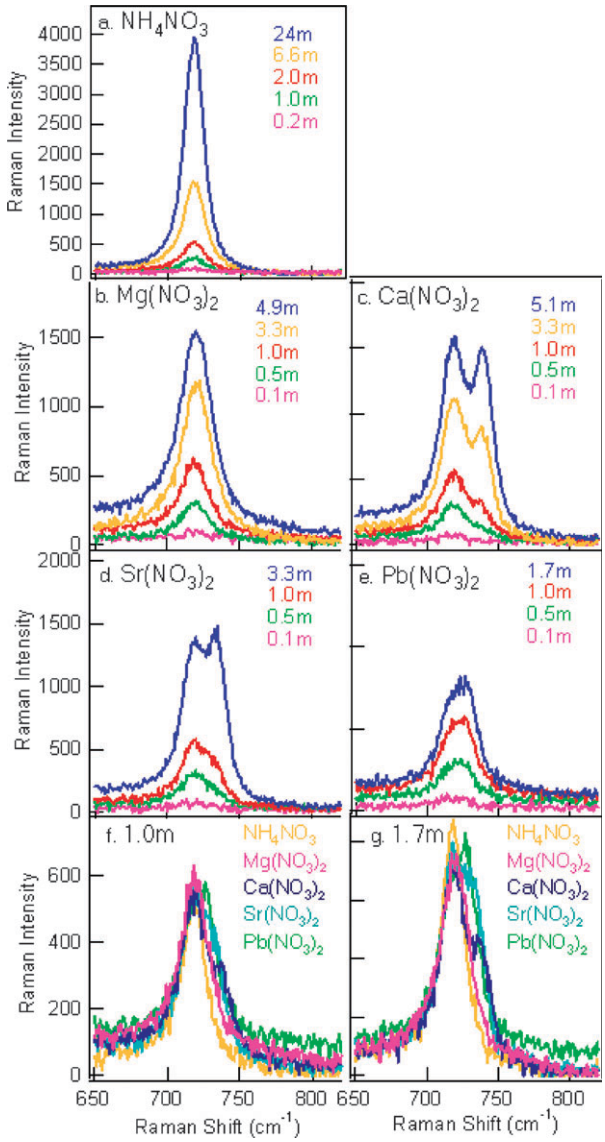

Fig. 2 Raman spectra of in-plane deformation modes: (a) NH_4NO_3 solutions; (b) $Mg(NO_3)_2$ solutions; (c) $Ca(NO_3)_2$ solutions; (d) $Sr(NO_3)_2$ solutions; (e) $Pb(NO_3)_2$ solutions; (f) 1.0 m solutions; (g) 1.7 m solutions. In panel (f) and (g), NH_4NO_3 has the same nitrate concentrations with other nitrate solutions, *i.e.* 2.0 m and 3.4 m, respectively.

our Raman results. This phenomenon is associated with the comparable strengths of the perturbation from NH_4^+ cations and from water molecules on nitrate anions. In dilute NH_4NO_3 aqueous solutions where the perturbation of NH_4^+ on nitrate is negligible, the hydrating water molecules interact with nitrate anions directly. In concentrated NH_4NO_3 solutions, one or more nitrate hydrating water molecules are replaced by NH_4^+ cations, and NH_4^+ and nitrate are in direct contact. The strength of the NH_4^+–NO_3^- interaction is however similar to the strength of the NO_3^-–water interaction. The similarity of NH_4^+ ions and water molecules has been reflected in many properties of aqueous ammonium salt solutions based on previous studies.[41–45] NH_4^+ ions fit well in the structure of liquid water and form hydrogen bonds of about the same strength as water molecules.[42,45] Compared to other monovalent metallic cation salts, ammonium salts produce the smallest change in viscosity, entropy, and proton resonance of liquid water.[42–44] Due to the similarity of NH_4^+ ions and water molecules, it is not surprising to observe similar strengths of the NH_4^+–NO_3^- interaction and the NO_3^-–water interaction, as shown in our Raman results.

As for $Mg(NO_3)_2$ solutions, spectra in Fig. 2b show no obvious peak splitting of the IPD band in our concentration range, suggesting a low degree of contact ion pairing or a weak perturbation of Mg^{2+} cations on nitrate anions in $Mg(NO_3)_2$ solutions.[20,40] Yet, the IPD band is not sensitive enough to differentiate between these two possibilities. The intermolecular Mg^{2+}–OH_2 stretching band discussed in section 3.1.4 clarifies the lack of contact ion pair formation in the $Mg(NO_3)_2$ aqueous solutions.

In the aqueous solutions of $Ca(NO_3)_2$, $Sr(NO_3)_2$, and $Pb(NO_3)_2$ (Fig. 2c–e) for concentrations lower than 0.50 m (0.0089 x), nitrate exhibits a single band at 720 ± 1 cm^{-1}. The single IPD peak for these low concentrations implies a low degree of contact ion pairing. As the concentration increases to 1.0 m (0.018 x), a shoulder appears at 738 cm^{-1}, 732 cm^{-1} and 728 cm^{-1} for $Ca(NO_3)_2$, $Sr(NO_3)_2$, and $Pb(NO_3)_2$, respectively (Fig. 2c–f). By further increasing the concentration, this high frequency shoulder gradually increases in intensity, and shifts to higher frequency. Notice here the high frequency side of the IPD band for $Pb(NO_3)_2$ is at a lower frequency compared to $Ca(NO_3)_2$ and $Sr(NO_3)_2$ (729 cm^{-1} *versus* 740 cm^{-1} and 735 cm^{-1} in concentrated solutions, for example). This may reflect differences in the polarizing power of the cations.[4] The value of 729 cm^{-1} is still within the range assigned to contact ion pairs in aqueous solutions. Therefore, we assign the high frequency component peak at 728–740 cm^{-1} to contact ion paired nitrate ions, and the low frequency component peak at ~718 cm^{-1} to hydrated nitrate ions and to solvent-shared, solvent-separated ion pairs where the cation perturbation is relatively weak compared to contact ion pairs. Since the majority of the contact ion pairs are associated with the high frequency component peak at 728–740 cm^{-1}, further discussion only considers this high frequency component peak as contact ion paired nitrate.

Fig. 3a shows the relative peak intensity of the contact ion paired nitrate (the ratio of the intensity of the ~740 cm^{-1} peak to the sum intensity of the ~720 cm^{-1} peak and the ~740 cm^{-1} peak, I_{CIP}/I_{total}) as a function of concentration in molality (units of moles per kg water) for different metal–nitrate aqueous solutions. The relative peak intensity has been used to estimate the percentage of the contact ion paired species in previous studies, assuming that the molar Raman intensity remains the same for free and ion paired forms of nitrate.[4,19] Fig. 3b reveals a linear correlation between the sum intensity of the nitrate IPD bands and the molarity (units of moles per litre water). Molarity units are more easily evaluated in this case because Raman spectroscopy probes a fixed volume, not a fixed mass. Therefore, the linearity of Fig. 3b indicates that the IPD intensity is not significantly sensitive to the relative amount of free or ion paired species, and that the assumption used by Fleissner *et al.*[4] is reasonable. The relative amount of the contact ion paired nitrate species is then

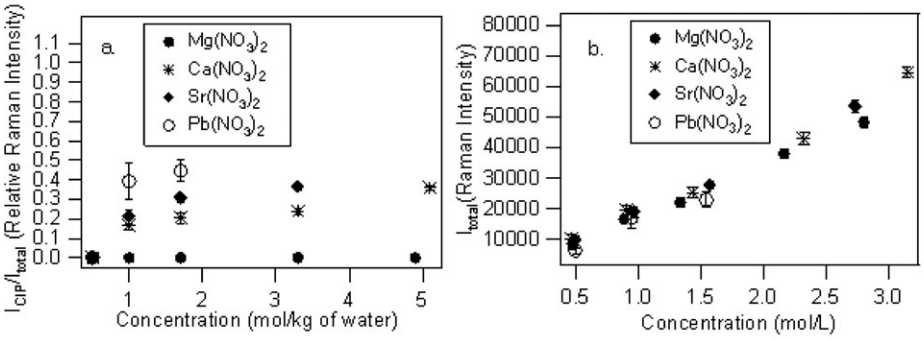

Fig. 3 Raman intensities of in-plane deformation modes as a function of concentration: (a) relative intensity of the contact ion paired nitrate as a function of molality; (b) sum intensity of the free and ion paired nitrate as a function of molarity.

extracted from Fig. 3a. For example, at concentration 3.3 m (0.056 *x*) there are 24% contact ion paired nitrate and 76% hydrated (may include ion paired) nitrate in the $Ca(NO_3)_2$ solution. This is consistent with Irish and Walrafen.[21] When comparing different nitrate solutions with the same concentration, the degree of contact ion pairing follows: $Pb(NO_3)_2 > Sr(NO_3)_2 > Ca(NO_3)_2 > Mg(NO_3)_2$. For instance, at concentration 1.7 m (0.030 *x*), 45% of nitrate in the $Pb(NO_3)_2$ solution is contact ion paired, and this number decreases to 31% for $Sr(NO_3)_2$, 20% for $Ca(NO_3)_2$, and 0% for $Mg(NO_3)_2$. The trend for $Sr(NO_3)_2$, $Ca(NO_3)_2$ and $Mg(NO_3)_2$ in aqueous solutions is consistent with Chang and Irish's studies,[20,21] though in the glassy state the trend has been found to be $Sr(NO_3)_2 > Ca(NO_3)_2 \approx Mg(NO_3)_2$.[4]

3.1.2 Symmetric stretch. The variation of the fwhm and the frequency of the nitrate SS band indicates the perturbation of metal cations on nitrate anions. Fig. 4 shows the Raman spectra of the nitrate SS modes. As concentration increases from 0.50 m (0.0089 *x*) to near saturation, the fwhm of the nitrate SS band increases from 10% to 20% relative to the lowest concentration SS modes (Fig. 4b–e). For comparison, in the case of NH_4NO_3 aqueous solutions, the SS fwhm variation is below 5% (Fig. 4a) (detailed fwhm values from Fig. 4 are shown in ESI)†. Vollmar[45] has suggested that the increase in the fwhm is caused by the breaking down of the solution structure, creating a more variable environment for the nitrate ions. In studies of $Zn(NO_3)_2$ at high temperatures and pressures,[19,46] it has been proposed that the bound (ion-paired) nitrate species relaxes (dampens) faster than the free species, resulting in a larger bandwidth of the bound species. The increase in bandwidth (Fig. 4a–e) therefore can be explained by the interaction of the cation with the nitrate anion.

Nitrate and its counter cation have a stronger tendency to form ion pairs at higher concentrations, affecting the fwhm of the SS. Consequently, the faster vibrational relaxation caused by the long-range Coulombic perturbation broadens the SS band. When comparing different nitrate solutions with the same nitrate concentration (Fig. 4f and g), the fwhm follows a trend $Pb(NO_3)_2 > Sr(NO_3)_2 \approx Ca(NO_3)_2 > Mg(NO_3)_2 > NH_4NO_3$. For instance, the fwhms are 13.0 cm^{-1}, 11.1 cm^{-1}, 11.0 cm^{-1}, 10.5 cm^{-1} and 8.0 cm^{-1} for $Pb(NO_3)_2$, $Sr(NO_3)_2$, $Ca(NO_3)_2$, $Mg(NO_3)_2$ and NH_4NO_3, respectively at 1.7 m (0.030 *x*) (NH_4NO_3 has a concentration of 3.4 m). This trend implies strong Coulombic effects of Pb^{2+} on nitrate relative to Sr^{2+}, Ca^{2+}, Mg^{2+}, and NH_4^+.

Peak position of the nitrate SS modes is also concentration dependent and cation dependent. For $Mg(NO_3)_2$, $Ca(NO_3)_2$, and $Sr(NO_3)_2$ aqueous solutions, the frequency slightly blue shifts from 1049 cm^{-1} at 0.10 m (0.0018 *x*) to 1050 cm^{-1} at concentrated concentrations (Fig. 4b–d). Interestingly, the SS frequency red shifts as concentration increases in $Pb(NO_3)_2$ solutions (Fig. 4e). Similar shifts of the SS band are observed in the infrared spectra (ESI)†. The peak position of $Pb(NO_3)_2$ is always at a lower frequency compared to other cations at the same concentration (Fig. 4f and g).

The blue shift of the SS band for $Mg(NO_3)_2$, $Ca(NO_3)_2$, and $Sr(NO_3)_2$ and the red shift for $Pb(NO_3)_2$ can be interpreted by two competitive forces: the weakening of the nitrate–water hydrogen bonding that causes a SS blue shift, and the ion pairing between cation and nitrate that results in a red shift of the SS. On one hand, metal cations in aqueous solutions interact with or even replace water molecules around nitrate, resulting in a weakening of the nitrate–water hydrogen bonding. Nitrate–water hydrogen bonding (water solvation) decreases the frequency of the nitrate SS vibration,[45] and thus the weakening of the nitrate–water hydrogen bonding leads to a blue shift of the nitrate SS band. On the other hand, the strong cation–nitrate interaction weakens the covalent N–O bond, and causes a red shift of the nitrate SS band.[46] It is the relative strengths of these two competitive effects that dictate the direction of the frequency shift of the nitrate SS band.

In the case of $Mg(NO_3)_2$, $Ca(NO_3)_2$, and $Sr(NO_3)_2$ solutions, the effects of weakening nitrate–water hydrogen bonding dominate. Consequently, the nitrate SS band blue shifts as concentration increases in their respective aqueous solutions. This is consistent with similar frequency shifts observed in previous studies of nitrate and sulfate.[4,38,45,47–49] For $Pb(NO_3)_2$ aqueous solutions, however, the effects from metal–nitrate interactions dominate. Having a large ionic radius and a relatively small surface charge density, Pb^{2+} binds water molecules relatively loosely compared to other metal cations examined in this study. The Coulombic perturbation of Pb^{2+} on nitrate exceeds the effect of nitrate–water hydrogen bond weakening. Similar red shifts have been observed for $Pb(NO_3)_2$-*N*-methylacetamide solutions and $Zn(NO_3)_2$ aqueous solutions.[18,19,46]

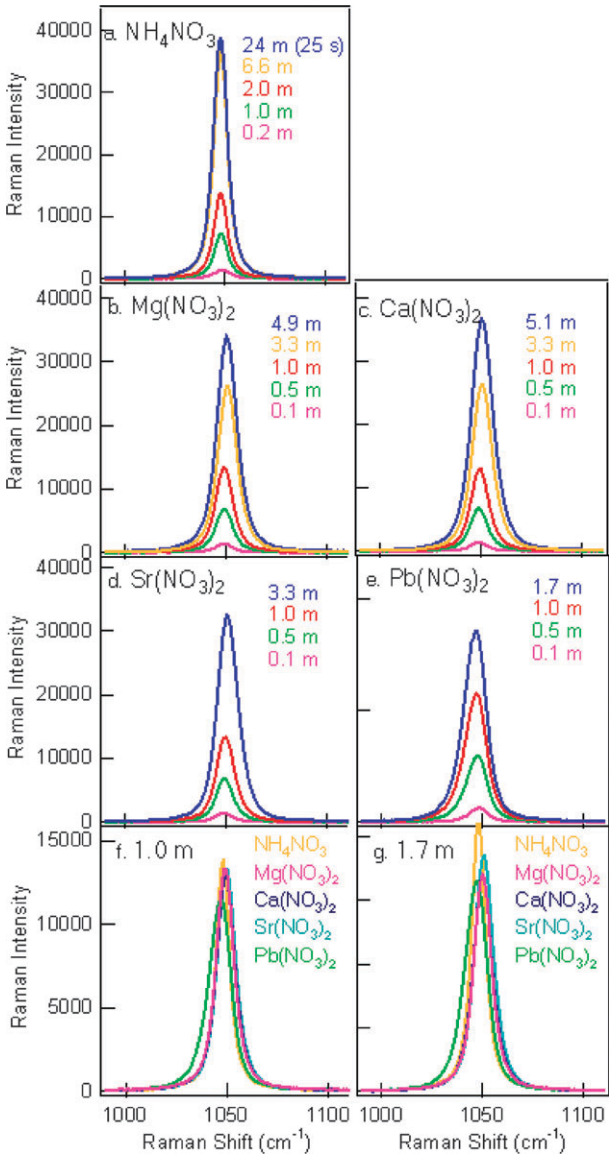

Fig. 4 Raman spectra of symmetric stretching modes: (a) NH_4NO_3 solutions; (b) $Mg(NO_3)_2$ solutions; (c) $Ca(NO_3)_2$ solutions; (d) $Sr(NO_3)_2$ solutions; (e) $Pb(NO_3)_2$ solutions; (f) 1.0 m solutions; (g) 1.7 m solutions. In panel (a), exposure time 25 s instead of 50 s was used for 24 m NH_4NO_3 because of detector saturation. In panel (f) and (g), NH_4NO_3 has the same nitrate concentrations as other nitrate solutions, *i.e.* 2.0 m and 3.4 m, respectively.

In the case of $NaNO_3$, though the surface charge density of Na^+ is smaller than that of Pb^{2+} (0.76 *vs.* 1.12), a blue shift rather than a red shift is observed (see ESI† for Raman spectra of $NaNO_3$). This phenomenon reflects the differences between monovalent and divalent metal ions. Low surface charge density of Na^+ leads to weak Na^+–water binding. Meanwhile, the Na^+–nitrate interaction is even weaker as a result of the single charge of sodium cations.

3.1.3 Asymmetric stretch. Unperturbed nitrate gives rise to a single asymmetric stretching $\nu_3(E')$ band at $\sim$1370 cm^{-1}.[13,15,40] In the aqueous nitrate solutions, two AS component peaks are observed, as shown in Fig. 5a–g. The degeneracy of the AS is caused by perturbation from water molecules as well as long-range Coulombic perturbation from cations.[15,18,38–40] *Ab initio* calculations on isolated complexes of nitrate ion with a single water molecule have identified two structures with C_{2v} and C_s symmetries. In both symmetries the two component peaks of the AS are separated by 40 to 50 cm^{-1}, which is consistent with the splitting in dilute aqueous solutions detected by previous experimental studies.[13,50,51] In the present study, the separation of the two component peaks varies from 63 cm^{-1} for 0.50 m $Mg(NO_3)_2$ (0.0089 *x*) to 90 cm^{-1} for saturated $Pb(NO_3)_2$ (see Fig. 5a–g; detailed peak separation values are shown in ESI†), suggesting Coulombic effects between the cation and nitrate. (In the aqueous solutions of NH_4NO_3, the separation is in the range 63 to 69 cm^{-1}, which suggests that the perturbation caused by water molecules and that caused by NH_4^+ cations are not exactly the same but similar in strength.) Although the effects of water molecules on nitrate ions vary in different systems, considering the magnitude of the difference in peak separation, we conclude that Pb^{2+} has the strongest tendency to form ion pairs with nitrate compared to the other cations since $Pb(NO_3)_2$ has the largest peak separation among these metal–nitrate solutions (Fig. 5f and g). This conclusion is consistent with the results from the IPD and the SS modes discussed above.

3.1.4 Intermolecular Mg^{2+}–OH_2 stretch. The intermolecular metal–water stretching bands are shown in Fig. 1a and 6. As shown in Fig. 1a, only in the Raman spectrum of the $Mg(NO_3)_2$ aqueous solution, the intermolecular Mg^{2+}–OH_2 band at $\sim$360 cm^{-1} predominates, indicating strong hydration of Mg^{2+} cations relative to other cations. The Raman spectra of the Mg^{2+}–OH_2 band at different $Mg(NO_3)_2$ concentrations were obtained and are shown in Fig. 6. Fig. 7 illustrates the curve-fitting results of these Mg^{2+}–OH_2 Raman spectra. Fig. 7a reveals a linear correlation between the peak intensity of the Mg^{2+}–OH_2 band and the molarity of the $Mg(NO_3)_2$ aqueous solution. The linearity indicates that there is no replacement of Mg^{2+} hydration water molecules by nitrate anions in our concentration range. Mg^{2+} cations retain their six-water primary solvation shells. Additionally, the peak position of the Mg^{2+}–OH_2 band remains constant with varying concentrations, as shown in Fig. 7b. This confirms that Mg^{2+} always retains its primary solvation shell and that the hydrated ions of $Mg(H_2O)_6^{2+}$ are very stable. Therefore, it is concluded that no contact ion pairing between Mg^{2+} and nitrate occurs in the aqueous solutions of $Mg(NO_3)_2$.

Hydration by water molecules competes with cation–anion ion pairing.[3,48,52] Having a small ionic radius and a large surface charge density, Mg^{2+} binds to water molecules tightly compared to other cations. It is difficult for nitrate anions to enter the first solvation shell of Mg^{2+} cations. Water molecules of the Mg^{2+} hydration shell compete against the nitrate anion more successfully. As a result, no contact ion pairing is present in the $Mg(NO_3)_2$ aqueous solutions. This is indicated by both the Raman IPD modes and the Mg^{2+}–OH_2 modes.

3.2 Free energy profiles

Fig. 8 illustrates the free energy profiles of $MgNO_3^+$, $CaNO_3^+$, $SrNO_3^+$, and $PbNO_3^+$ at infinite dilution. There are three distinct minima in each free energy profile. The first

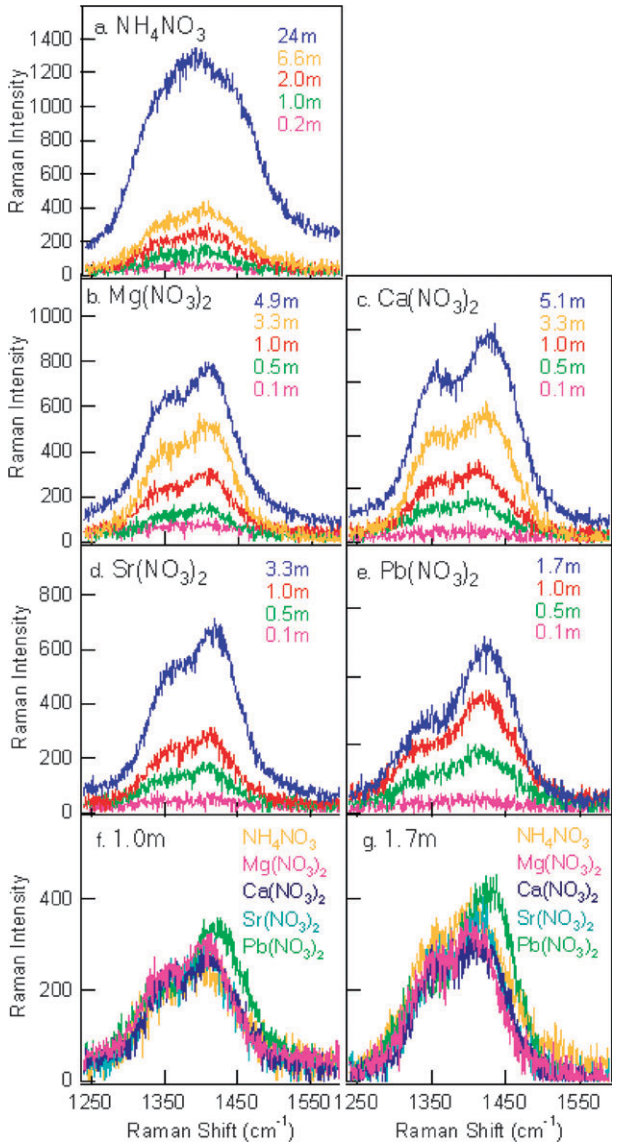

Fig. 5 Raman spectra of asymmetric stretching modes: (a) NH_4NO_3 solutions; (b) $Mg(NO_3)_2$ solutions; (c) $Ca(NO_3)_2$ solutions; (d) $Sr(NO_3)_2$ solutions; (e) $Pb(NO_3)_2$ solutions; (f) 1.0 m solutions; (g) 1.7 m solutions. In panel (f) and (g), NH_4NO_3 has the same nitrate concentrations with other nitrate solutions, *i.e.* 2.0 m and 3.4 m, respectively.

minima at 3.25 Å, 3.40 Å, 3.85 Å, and 3.90 Å for $MgNO_3^+$, $CaNO_3^+$, $SrNO_3^+$, and $PbNO_3^+$, respectively, correspond to contact ion pair formation, the second minima at 5.20 Å for $MgNO_3^+$ and $CaNO_3^+$, 5.60 Å for $SrNO_3^+$, and 5.80 Å for $PbNO_3^+$ refer to the solvent-shared ion pair, and the third minima at 7.30 Å for $MgNO_3^+$ and $CaNO_3^+$, and 7.80 Å for $SrNO_3^+$ and $PbNO_3^+$, correspond to the solvent-separated ion pair. For each minimum and maximum in the free energy profile, we examined the proximity of the free nitrate anion to the constrained ion pair, and found that the free nitrate anion did not form a stable complex with the ion pair during the timeframe of the simulations. According to the free energy profile for $MgNO_3^+$, the formation of contact ion pairs between Mg^{2+} cations and nitrate anions is extremely unfavorable since the free energy minimum for contact ion pairing is significantly higher (>9 kcal mol^{-1}) than those for solvent-shared and solvent-separated ion pairing. In addition, the free energy minimum for the solvent-shared ion pair formation is slightly lower than that for the solvent-separated ion pair formation, suggesting that the solvent-shared ion pair is the most stable ion pair in $Mg(NO_3)_2$ solutions.

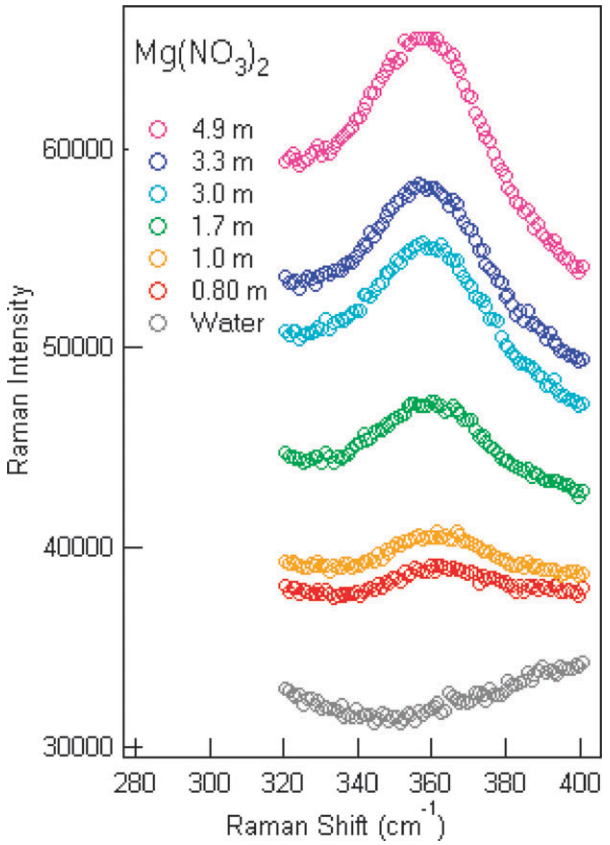

Fig. 6 Raman spectra of Mg^{2+}–OH_2 stretching modes of $Mg(NO_3)_2$ aqueous solutions.

Fig. 9 illustrates the orientation of the nitrate ion with respect to Mg^{2+} for the contact ion pair, solvent-shared ion pair, and solvent-separated ion pair configurations. For the contact ion pair (Fig. 9a), one oxygen atom of the nitrate ion is pointed towards Mg^{2+}. The nitrate ion replaces one of the six water molecules ordinarily found in the first hydration shell of Mg^{2+}. Given the extremely large free energy barrier associated with removing a water molecule from this hydration shell of Mg^{2+}, this complex is unlikely to form. For the solvent-shared ion pair (Fig. 9b), two of the nitrate oxygen atoms are closer to Mg^{2+} than the nitrogen atom. In the Mg^{2+}–NO_3^- solvent-separated ion pair (Fig. 9c), the nitrate orientation with respect to Mg^{2+} varies between having one or two oxygen atoms nearer to Mg^{2+} than nitrogen. The distance between the ions allows for two water molecules between them, one that forms a hydrogen bond to the nitrate anion and one that is part of the first hydration shell around Mg^{2+}.

For $CaNO_3^+$, the free energy profile shown in Fig. 8 indicates that contact ion pairing is thermodynamically preferred over solvent-shared or solvent-separated ion pairing. The $SrNO_3^+$ and $PbNO_3^+$ free energy profiles are comparable to $CaNO_3^+$,

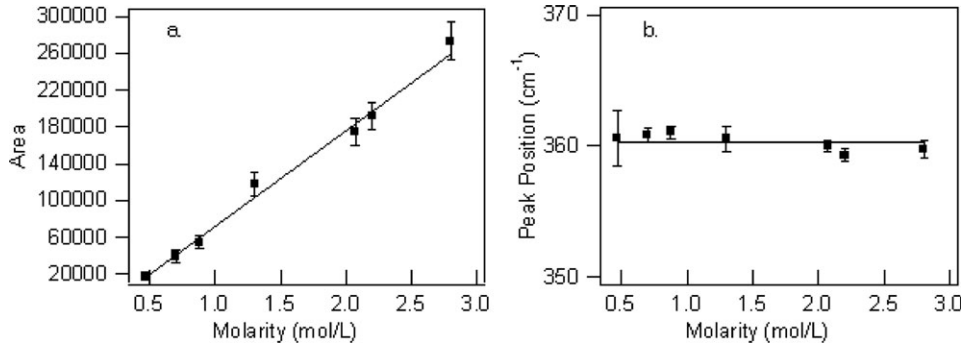

Fig. 7 (a) Raman intensities of Mg^{2+}–OH_2 stretching modes as a function of concentration; (b) Raman frequencies of Mg^{2+}–OH_2 stretching modes as a function of concentration.

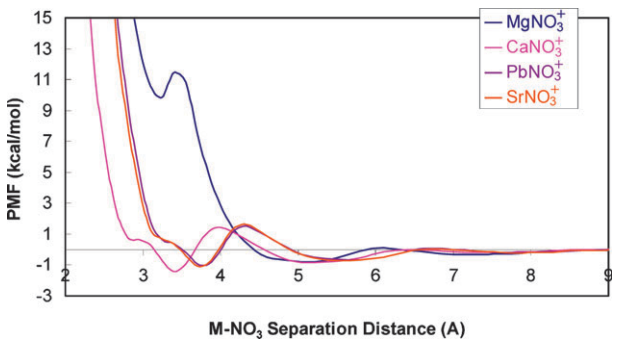

Fig. 8 Free energy profiles (potential-of-mean-force (PMF)) of $MgNO_3^+$, $CaNO_3^+$, $PbNO_3^+$, and $SrNO_3^+$ at infinite dilution.

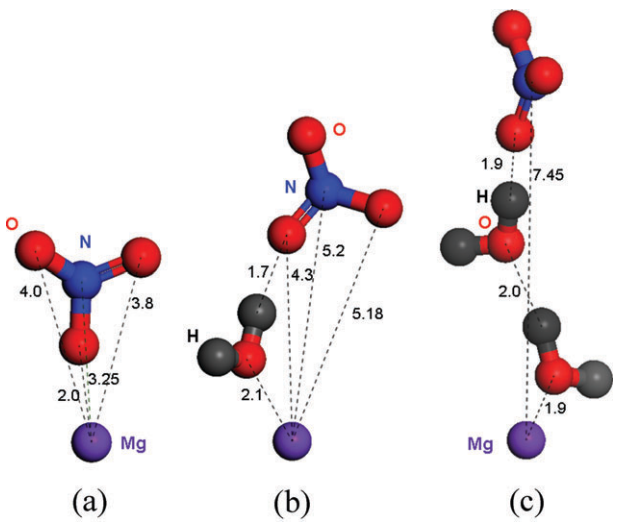

Fig. 9 Structures for $MgNO_3^+$: (a) contact ion pair (improbable); (b) solvent-shared ion pair; (c) solvent-separated ion pair.

but shifted by ~0.5 Å. All three of these free energy profiles exhibit a shoulder or inflection point as the ion pair separation distance is brought closer than the preferred contact ion pair distance. These inflections reflect changes in the nitrate orientation relative to the divalent metal cation. The water molecules in the hydration shells around Ca^{2+}, Sr^{2+}, and Pb^{2+} are less tightly bound to the cation than the water molecules around Mg^{2+}. Therefore, more of the nitrate oxygen atoms can readily exchange for the water oxygens in the first shell around these

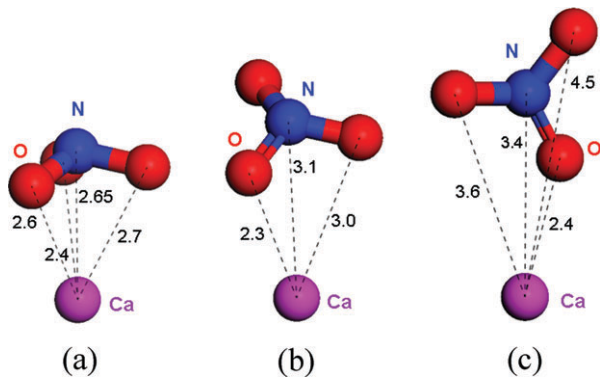

Fig. 10 Structures of $CaNO_3^+$ at Ca–N distances of (a) 2.65 Å, (b) 3.1 Å, and (c) 3.4 Å; (c) corresponds to the contact ion pair minimum.

metal cations than around Mg^{2+}. For example, the nitrate oxygen atoms in the Ca^{2+}–NO_3^- ion pair, are essentially equidistant to the cation at a constraint distance of 2.65 Å (Fig. 10a), and substitute for several water oxygens in the first coordination sphere of Ca^{2+}. The average number of water molecules in this shell is 5.4; the three nitrate oxygen atoms complete the shell such that Ca^{2+} is immediately surrounded by approximately eight negatively-charged oxygen moieties. The nitrate ion is highly distorted and non-planar, leading to an unfavorable structure and orientation. At a Ca–N distance of 3.1 Å, only two of the three O atoms coordinate with Ca^{2+}, while the 3rd oxygen atom points away from the cation (Fig. 10b). The number of water molecules in the first coordination sphere for Ca^{2+} is now 6.1. At 3.4 Å, the most favorable contact ion pair distance, only one of the nitrate oxygen atoms is in the first coordination sphere (Fig. 10c), along with approximately 7 water oxygen atoms. This ion pair structure is similar to that calculated for $MgNO_3^+$. In both solvent-shared and solvent-separated ion pair structures, Ca^{2+} is hydrated by an average of 7.6 water molecules as in bulk solution. The ion pair structures and changes in hydration number calculated for $SrNO_3^+$ and $PbNO_3^+$ as a function of cation–anion distance are analogous to those observed for $CaNO_3^+$.

4. Conclusions

Studies of aqueous solutions of $Mg(NO_3)_2$, $Ca(NO_3)_2$, $Sr(NO_3)_2$, and $Pb(NO_3)_2$ were carried out using Raman

spectroscopy and molecular dynamics simulations. The perturbation of metal–nitrate ion pairing and water hydration lowers the symmetry of nitrate. Therefore peak shifting, splitting and broadening are observed in the Raman spectra of the nitrate aqueous solutions. Analysis of the spectral features reveals that Pb^{2+} has a strong tendency to form ion pairs with nitrate relative to Sr^{2+}, Ca^{2+}, and Mg^{2+}, and contact ion pair formation decreases with decreasing cation size and increasing cation charge density: $Pb^{2+} > Sr^{2+} > Ca^{2+} > Mg^{2+}$. The formation of contact ion pairs in the aqueous solutions of $Mg(NO_3)_2$ is significantly different from other nitrate salt solutions. The strong Mg^{2+}–OH_2 mode is observed spectroscopically. Free energy profiles indicate that there is a large activation barrier to remove water from the first hydration shell of Mg^{2+} and to form a contact ion pair, and thus the formation of contact ion pairs in $Mg(NO_3)_2$ solutions is thermodynamically unfavorable. In $Ca(NO_3)_2$, $Sr(NO_3)_2$, and $Pb(NO_3)_2$ aqueous solutions, however, because of the low free energy of the contact ion pair formation, contact ion pairing is thermodynamically preferred over solvent-shared and solvent-separated ion pairing. The most favorable orientation of metal–nitrate contact ion pairs is with one of the nitrate oxygen atoms pointing towards the divalent metal cation.

Acknowledgements

The authors thank Nathan Gaubert for determination of the Raman system resolution. We gratefully acknowledge funding for this work from the US Department of Energy Office of Basic Energy Sciences, Division of Chemical Sciences, Geosciences, and Biosciences both at SNL and at OSU (DOE-BES, DE-FG02-04ER15495). Sandia National Laboratories is a multi-program laboratory operated by the Sandia Corporation, a Lockheed Martin Company for the United States Department of Energy's National Nuclear Security Administration under Contract DE-AC04-94AL85000.

References

1. Y. Marcus and G. Hefter, *Chem. Rev*., 2006, **106**, 4585–4621.
2. R. Buchner, T. Chen and G. Hefter, *J. Phys. Chem. B*, 2004, **108**, 2365–2375.
3. K. D. Collins, *Biophys. J*., 1997, **72**, 65–76.
4. G. Fleissner, A. Hallbrucker and E. Mayer, *J. Phys. Chem*., 1993, **97**, 4806–4814.
5. B. Minofar, R. Vacha, A. Wahab, S. Mahiuddin, W. Kunz and P. Jungwirth, *J. Phys. Chem. B*, 2006, **2006**, 15939–15944.
6. Y. Marcus, *Ion Solvation*, Wiley, Chichester, UK, 1985.
7. M. R. Hoffmann, A. Laskin and B. J. Finlayson-Pitts, *J. Aerosol Sci*., 2004, **35**, 869–887.
8. C. S. Boxe, A. J. Colussi, M. R. Hoffmann, I. M. Perez, J. G. Murphy and R. C. Cohen, *J. Phys. Chem. A*, 2006, **110**, 3578–3583.
9. L. X. Dang, T.-M. Chang, M. Roeselova, B. C. Garrett and D. J. Tobias, *J. Chem. Phys*., 2006, **124**, 066101.
10. J. L. Thomas, M. Roeselova, L. X. Dang and D. J. Tobias, *J. Phys. Chem. A*, 2007, **111**, 3091–3098.
11. D. E. Irish, A. R. Davis and R. A. Plane, *J. Chem. Phys*., 1969, **50**, 2262–2263.
12. G. Fleissner, A. Hallbrucker and E. Mayer, *Chem. Phys. Lett*., 1994, **218**, 93–99.
13. M. R. Waterland, D. Stockwell and A. M. Kelley, *J. Chem. Phys*., 2001, **114**, 6249–6258.
14. R. E. Hester and R. A. Plane, *J. Chem. Phys*., 1964, **40**, 411–414.
15. M. Peleg, *J. Phys. Chem*., 1972, **76**, 1019–1025.
16. P. Smirnov, M. Yamagami, H. Wakita and T. Yamaguchi, *J. Mol. Liq*., 1997, **73/74**, 305–316.
17. N. Rohman, A. Wahab and S. Mahiuddin, *J. Solution Chem*., 2005, **34**, 77–94.
18. D. E. Irish, T. G. Chang and S.-Y. Tang, *J. Phys. Chem*., 1981, **85**, 1686–1692.
19. P. D. Spohn and T. B. Brill, *J. Phys. Chem*., 1989, **93**, 6224–6231.
20. T. G. Chang and D. E. Irish, *J. Phys. Chem*., 1973, **77**, 52–57.
21. D. E. Irish and G. E. Walrafen, *J. Chem. Phys*., 1967, **46**, 378–384.
22. M. Xu, K. M. Callahan, C. Y. Tang, D. J. Tobias and H. C. Allen, *J. Phys. Chem*., 2008, submitted.
23. M. Xu, K. M. Callahan, R. Spinney, D. J. Tobias and H. C. Allen, 2008, in preparation.
24. R. L. Frost and D. W. James, *J. Chem. Soc., Faraday Trans. 1*, 1982, **78**, 3235–3247.
25. R. L. McCreery, *Raman Spectroscopy for Chemical Analysis*, John Wiley & Sons, New York, 2000.
26. D. Trzesniak, A.-P. E. Kunz and W. F. van Gunsteren, *ChemPhysChem*, 2007, **8**, 162–169.
27. A. A. Chialvo, P. T. Cummings, H. D. Cochran, J. M. Simonson and R. E. Mesmer, *J. Chem. Phys*., 1995, **103**, 9379–9387.
28. G. Ciccotti, M. Ferrario, J. T. Hynes and R. Kapral, *Chem. Phys*., 1989, **129**, 241–251.
29. E. Guardia, R. Rev and J. A. Padro, *Chem. Phys*., 1991, **155**, 187–195.
30. J.-P. Ryckaert, G. Ciccotti and H. J. C. Berendsen, *J. Comput. Phys*., 1977, **23**, 327–341.
31. S. Plimpton, *J. Comput. Phys*., 1995, **117**, 1–19.
32. S. Plimpton, R. Pollock and M. Stevens, Eighth SIAM Conference on Parallel Processing for Scientific Computing, 1997.
33. H. J. C. Berendsen, J. P. M. Postma, W. F. van Gunsteren and J. Hermans, in *Intermolecular Forces*, ed. B Pullman, D. Reidel Publishing Co., Dordrecht, 1981.
34. O. Teleman, B. Jonsson and S. Engstrom, *Mol. Phys*., 1987, **60**, 193–203.
35. J. Åqvist, *J. Phys. Chem*., 1990, **94**, 8021–8024.
36. C. Cadena and E. J. Maginn, *J. Phys. Chem. B*, 2006, **110**, 18026–18039.
37. R. E. Hester and R. A. Plane, *J. Chem. Phys*., 1966, **45**, 4588–4593.
38. A. Wahab, S. Mahiuddin, G. Hefter, W. Kunz, B. Minofar and P. Jungwirth, *J. Phys. Chem. B*, 2005, **109**, 24108–24120.
39. D. E. Irish and A. R. Davis, *Can. J. Chem*., 1968, **46**, 943–951.
40. D. E. Irish, G. Chang and D. L. Nelson, *Inorg. Chem*., 1970, **9**, 425–426.
41. K. Fajans and O. Johnson, *J. Am. Chem. Soc*., 1942, **64**, 668–678.
42. H. S. Frank and A. L. Robinson, *J. Chem. Phys*., 1940, **8**, 933–938.
43. M. Kaminsky, *Discuss. Faraday Soc*., 1957, **24**, 171–179.
44. J. C. Hindman, *J. Chem. Phys*., 1962, **36**, 1000–1016.
45. P. M. Vollmar, *J. Chem. Phys*., 1963, **39**, 2236–2248.
46. Y. Ikushima, N. Saito and M. Arai, *J. Phys. Chem. B*, 1998, **102**, 3029–3035.
47. Y.-H. Zhang, M. Y. Choi and C. K. Chan, *J. Phys. Chem. A*, 2004, **108**, 1712–1718.
48. D. Watanabe and H. Hamaguchi, *J. Chem. Phys*., 2005, **123**, 34508.
49. H. S. Frank and W.-Y. Wen, *Discuss. Faraday Soc*., 1957, **24**, 133–140.
50. M. Shen, Y. Xie and H. F. Schaefer, *J. Chem. Phys*., 1990, **93**, 3379–3388.
51. M. R. Waterland and A. M. Kelley, *J. Chem. Phys*., 2000, **113**, 6760–6773.
52. M. Y. Kiriukhin and K. D. Collins, *Biophys. Chem*., 2002, **99**, 155–168.